Human PET Studies of Metabotropic Glutamate Receptor Subtype 5 with ^{11}C-ABP688

Simon M. Ametamey[1], Valerie Treyer[2], Johannes Streffer[3], Matthias T. Wyss[2], Mark Schmidt[4], Milen Blagoev[1], Samuel Hintermann[4], Yves Auberson[4], Fabrizio Gasparini[4], Uta C. Fischer[3], and Alfred Buck[2]

[1]Center for Radiopharmaceutical Science of ETH, PSI, and USZ, Department of Chemistry and Applied Biosciences of ETH, Zurich, Switzerland; [2]PET Center, Division of Nuclear Medicine, University of Zurich, Zurich, Switzerland; [3]Division of Psychiatric Research, University of Zurich, Zurich, Switzerland; and [4]Novartis Institutes for Biomedical Research Basel, Novartis Pharma AG, Basel, Switzerland

3-(6-Methyl-pyridin-2-ylethynyl)-cyclohex-2-enone-*O*-^{11}C-methyl-oxime (^{11}C-ABP688), a noncompetitive and highly selective antagonist for the metabotropic glutamate receptor subtype 5 (mGluR5), was evaluated for its potential as a PET agent. **Methods:** Six healthy male volunteers (mean age, 25 y; range, 21–33 y) were studied. Brain perfusion (^{15}O-H_2O) was measured immediately before each ^{11}C-ABP688 PET scan. For anatomic coregistration, T1-weighted MRI was performed on each subject. Arterial blood samples for the determination of the arterial input curve were obtained at predefined time points, and ^{11}C-ABP688 uptake was assessed quantitatively using a 2-tissue-compartment model. **Results:** An initial rapid uptake of radioactivity followed by a gradual clearance from all examined brain regions was observed. Relatively high radioactivity concentrations were observed in mGluR5-rich brain regions such as the anterior cingulate, medial temporal lobe, amygdala, caudate, and putamen, whereas radioactivity uptake in the cerebellum and white matter, regions known to contain low densities of mGluR5, was low. Specific distribution volume as an outcome measure of mGluR5 density in the various brain regions ranged from 5.45 ± 1.47 (anterior cingulate) to 1.91 ± 0.32 (cerebellum), and the rank order of the corresponding specific distribution volumes of ^{11}C-ABP688 in cortical regions was temporal > frontal > occipital > parietal. The metabolism of ^{11}C-ABP688 in plasma was rapid; at 60 min after injection, 25% ± 0.03% of radioactivity measured in the plasma of healthy volunteers was intact parent compound. **Conclusion:** The results of these studies indicate that ^{11}C-ABP688 has suitable characteristics and is a promising PET ligand for imaging mGluR5 distribution in humans. Furthermore, it could be of great value for the selection of appropriate doses of clinically relevant candidate drugs that bind to mGluR5 and for PET studies of patients with psychiatric and neurologic disorders.

Key Words: metabotropic glutamate receptor subtype 5; ^{11}C-ABP688; positron emission tomography; specific distribution volume

J Nucl Med 2007; 48:247–252

Received Sep. 5, 2006; revision accepted Nov. 3, 2006.

For correspondence or reprints contact: Simon M. Ametamey, PhD, Center for Radiopharmaceutical Science of ETH, PSI, and USZ, ETH-Hönggerberg, D-CHAB IPW HCI H427, Wolfgang-Pauli-Strasse 10, CH-8093 Zurich, Switzerland.

E-mail: simon.ametamey@pharma.ethz.ch

COPYRIGHT © 2007 by the Society of Nuclear Medicine, Inc.

Glutamate is considered the major excitatory neurotransmitter in the central nervous system. Metabotropic glutamate receptors (mGluRs) are G-protein–coupled receptors that activate intracellular secondary messenger systems when bound by the physiologic ligand glutamate. In the central nervous system, mGluRs modulate glutamatergic neurotransmission and are recognized potential therapeutic targets (*1,2*). Eight mGluR subtypes have been identified and classified into 3 groups. Group I mGluRs (mGluR1 and mGluR5) are coupled to phospholipase C and upregulate or downregulate neuronal excitability (*3*). Group II (mGluR2 and mGluR3) and group III (mGluR4, mGluR6, mGluR7, and mGluR8) inhibit adenylate cyclase and hence reduce synaptic transmission.

During the last few years, mGluRs have been the focus of intensive investigation. Their possible involvement in a variety of disease states (*2*), including anxiety (*4,5*), depression (*5*), schizophrenia (*6*), Parkinson's disease (*7*), drug addiction or withdrawal (*8*), and various pain states (*9–11*), has been reported.

Imaging techniques such as PET offer the possibility to visualize and study mGluR5 under physiologic and pathologic conditions. Although mGluR5 antagonists have been used successfully in vitro to label mGluR5 (*12,13*), imaging studies of mGluR5 have been hampered by the lack of a tracer that is suitable for in vivo imaging (*14–16*). Hamill et al. recently reported on the successful imaging of mGluR5 in a rhesus monkey brain with 3 different ligands (*17*), but no report on the human use of any of these tracers has yet been published. More recently, we reported on 3-(6-methyl-pyridin-2-ylethynyl)-cyclohex-2-enone-*O*-^{11}C-methyl-oxime (^{11}C-ABP688) (Fig. 1) as a potential PET agent for mGluR5 (*18*). Ex vivo and in vivo studies using rodents showed specific binding in mGluR5-rich brain regions—in contrast to the 3 ligands disclosed by Hamill et al. (*17*)—with negligible uptake in the cerebellum, a brain region known to be devoid of mGluR5. The specificity of ^{11}C-ABP688 binding to mGluR5 was further substantiated using mGluR5 knockout mice.

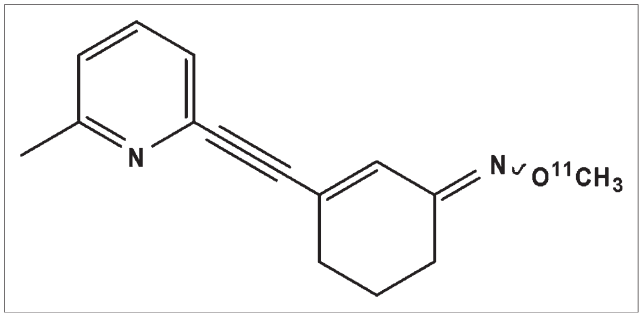

FIGURE 1. Structure of ^{11}C-ABP688.

The present study investigated the utility of ^{11}C-ABP688 for imaging mGluR5 in humans.

MATERIALS AND METHODS

Radiosynthesis of ^{11}C-ABP688

The ^{11}C labeling of ABP688 was achieved by O-^{11}C-methylation of desmethyl-ABP688 with ^{11}C-methyl iodide as described previously (*18*) but with slight modifications. Briefly, ^{11}C-methyl iodide was produced with a PET TRACE system (GE Healthcare) at the University Hospital in Zurich from ^{11}C-CO_2 in a 2-step reaction sequence involving catalytic reduction of ^{11}C-CO_2 to ^{11}C-methane and subsequent gas-phase iodination according to the standard procedure (*19*). In a typical procedure, the sodium salt of desmethyl-ABP688 obtained by stirring desmethyl-ABP688 with sodium hydride in anhydrous *N,N*-dimethylformamide was reacted with ^{11}C-methyl iodide at 90°C for 5 min and the product purified by semipreparative high-performance liquid chromatography (Luna C18 10-μm column [Phenomenex]; 250 × 10 mm; mobile phase, ethanol:0.1% phosphoric acid [50:50]; flow rate, 6 mL/min). The product peak was collected, passed through a Millex-FG sterile filter (Millipore), and formulated for human application.

Study Population

Six healthy male volunteers (mean age, 25 y; range, 21–33 y) were studied. None of the subjects had a history of neurologic or psychiatric disorders. The study was approved by the ethics committee of Canton Zurich, the Swiss Federal Office for Radiation Protection, and SwissMedic. Written consent was obtained from each volunteer.

MRI

For anatomic coregistration, a 3-dimensional spoiled gradient-echo T1-weighted whole-brain image (voxel size, 0.94 × 0.94 × 1.5 mm) was acquired for each subject on a 1.5-T Signa Infinity TwinSpeed MRI system (GE Healthcare).

PET

The PET studies were performed on a whole-body Discovery LS PET/CT scanner (GE Healthcare) in 3-dimensional mode. This is a scanner with an axial field of view of 14.6 cm and a reconstructed in-plane resolution of 7 mm. Before positioning of the volunteers on the scanner, catheters were placed in an antecubital vein for tracer injection and in the radial artery for blood sampling. Before the PET study, a low-dose CT scan was acquired for correction of photon attenuation.

Transaxial images of the brain were reconstructed using filtered backprojection (matrix, 128 × 128; 35 slices; voxel size, 2.34 × 2.34 × 4.25 mm).

^{15}O-H_2O PET. Before each study with ^{11}C-ABP688, cerebral perfusion (cerebral blood flow, or CBF) was evaluated using ^{15}O-H_2O. For each PET measurement, 400–500 MBq of ^{15}O-H_2O were injected intravenously using an automatic injection device that delivers a predefined dose of ^{15}O-H_2O over 20 s. After the bolus had arrived in the brain, a series of eighteen 10-s scans was initiated. The time course of arterial radioactivity was assessed by continuous sampling of blood drawn from the radial artery.

^{11}C-ABP688 PET. After injection of 300–350 MBq of radioligand as a slow bolus over 2 min, a series of 20 scans was initiated in 3-dimensional mode (10 × 60 s and 10 × 300 s; 60-min total study duration).

For determination of the arterial input curve, arterial blood samples were collected every 30 s for the first 6 min and then at increasing intervals until the end of the study (60 min after injection). An aliquot of each sample was measured in a γ-counter. Plasma samples were analyzed to correct for radiolabeled metabolites. Samples of plasma (200 μL) were diluted with 2.5 mL of water. For assessment of tracer–to–radiolabeled metabolite ratios, the solution was passed through Sep-Pak tC18 cartridges (Waters), and each was eluted with 5 mL of water. ^{11}C radioactivity trapped on the cartridges and aliquots of the eluted solution—corresponding to parent compound and radiolabeled metabolites, respectively—was measured in a γ-counter.

Data Analysis

All calculations were performed using the dedicated software PMOD (PMOD Technologies) (*20*). Decay-corrected time–activity curves were generated for the following cerebral regions: anterior cingulate, medial temporal lobe, parietal cortex, cerebellum, and white matter. Values for the specific distribution volume (DV) were calculated from the estimated rate constants.

^{15}O-H_2O PET. Quantitative parametric maps representing regional CBF were calculated using the integration method described by Alpert et al. (*21*).

^{11}C-ABP688 PET. Tissue time–activity curves were generated from various brain structures by applying manually drawn volumes of interest to the dynamic datasets. Two-tissue-compartment models were fitted to the time–activity curves, resulting in the rate constants K1, k2, k3, and k4. K1 is a rate constant describing the transfer of radioligand from plasma to the compartment consisting of free and nonspecifically bound ligand; k2 is a rate constant describing the reverse. The rate constants k3 and k4 denote radioligand binding to the receptor and dissociation from the receptor, respectively. The metabolite-corrected arterial activity was used as the input function for calculating the model curve, and least-squares optimization was performed using the Levenberg–Marquardt algorithm. Additionally, a voxelwise analysis was used to calculate quantitative maps of the model rate constants. To reduce the number of fit parameters, a global value of K1/k2 (nondisplaceable compartment) for a study was obtained in a first step by a coupled fit of the regional time–activity curves with K1/k2 as a common parameter (*22*). In a second step, the 2-tissue-compartment model was fitted to the time–activity curve of each individual voxel using the global K1/k2 value as a fixed model parameter (*23*). The specific DVs (K1/k2) × (k3/k4) served as the outcome parameter directly related to cerebral mGluR5 density. All data were processed using the quantitative PMOD software.

RESULTS

^{11}C-ABP688 was obtained from ^{11}C-methyl iodide with an overall decay-corrected radiochemical yield of 35% ± 8% (n = 14). The radiochemical purity was greater than 98%, and the specific radioactivity ranged from 70 to 95 GBq/μmol at the time of injection. The total amount of stable ABP688 in the formulated solution was always less than 5 μg.

In Figure 2 are shown mean parametric images of CBF, K1, and DVs, as well as anatomic MR images, obtained from the 6 subjects. Visual inspection of ^{15}O-H_2O perfusion images and the K1 images obtained from ^{11}C-ABP688 uptake reveal similar patterns. In Figure 3 are depicted representative time–activity curves of anterior cingulate, medial temporal lobe, parietal cortex, cerebellum, and white matter from a single subject. An initial rapid uptake of radioactivity followed by a gradual clearance from all regions was observed. Radioactivity peaked at 4 min after the start of the PET scan for all the brain regions examined, except the white matter. Arterial plasma radioactivity showed a typical shape, with a peak at 30–60 s that was followed by a rapid decline (data not shown). The metabolite-corrected plasma time–activity curve (input function) was used to calculate specific DVs from the region-of-interest–derived regional time–activity curve. Relatively high radioactivity concentrations were observed in mGluR5-rich brain regions such as the anterior cingulate, medial temporal lobe, amygdala, caudate, and putamen, whereas radioactivity uptake in the cerebellum and white matter, regions known to contain low densities of the mGluR5, was low. Preliminary kinetic analysis showed that radioactivity uptake across the brain regions, except the white matter, was best described by a 2-tissue-compartment model using the Akaike information criterion (*24*), F-statistics, and visual inspection of the residuals. Figure 4 depicts the results for several brain regions and their corresponding specific DVs. The rank order of binding of ^{11}C-ABP688 in cortical regions was temporal > frontal > occipital > parietal, and the outcome measures of mGluR5 density in the various brain regions ranged from 5.45 ± 1.47 (anterior cingulate) to 1.91 ± 0.32 (cerebellum).

Metabolism of ^{11}C-ABP688 was rapid. The percentages of radioactivity representing intact parent compound in plasma in the study subjects were 64 ± 0.08, 44 ± 0.10, 36 ± 0.08, 28 ± 0.03, 28 ± 0.04, and 25 ± 0.03 at 5, 10, 15, 30, 40, and 60 min, respectively. The extraction method used in this metabolite study proved suitable, because the recovery of radioactivity was greater than 92%.

DISCUSSION

To our knowledge, no clinically validated PET radioligand has been reported for the in vivo imaging of mGluR5. The aim of this present study was to evaluate the use of ^{11}C-ABP688 to label mGluR5 in human brain.

The results of the PET studies demonstrated a high initial brain uptake of ^{11}C-ABP688. Using the relation for the first-pass extraction fraction (K1/CBF) yielded an extraction fraction of 0.87 ± 0.21. This high brain uptake yielded high-quality images and favorable statistics for tracer kinetic modeling. As expected, visual inspection of the ^{15}O-H_2O perfusion images and K1 images obtained from ^{11}C-ABP688 uptake revealed similar patterns (Fig. 2). Indeed, the log D value of 2.4 for ^{11}C-ABP688 suggests that it should be sufficiently lipophilic for free diffusion through

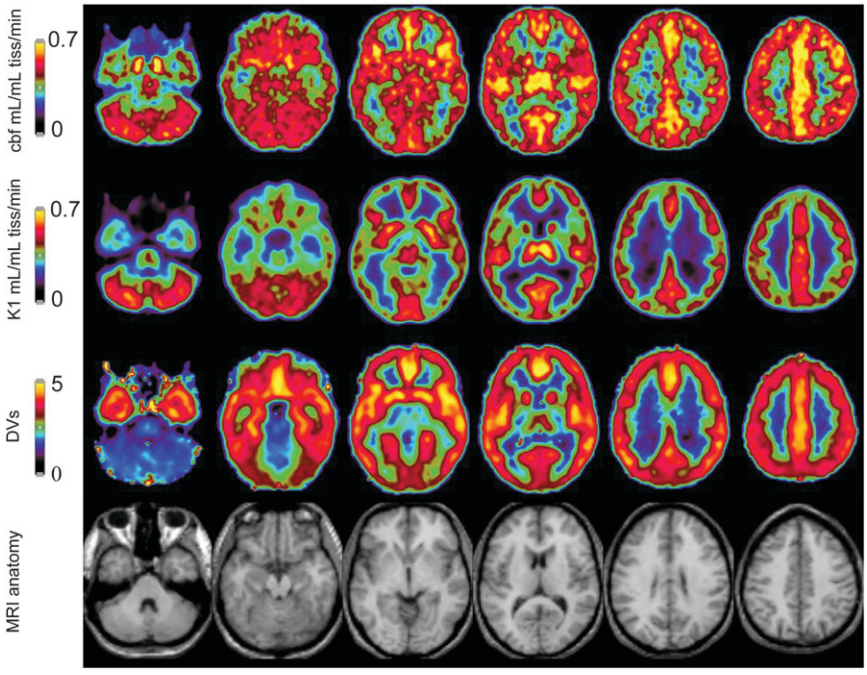

FIGURE 2. CBF, K1, DVs, and anatomic MR images. All images are displayed in stereotactic space and represent mean of 6 healthy volunteers. tiss = tissue.

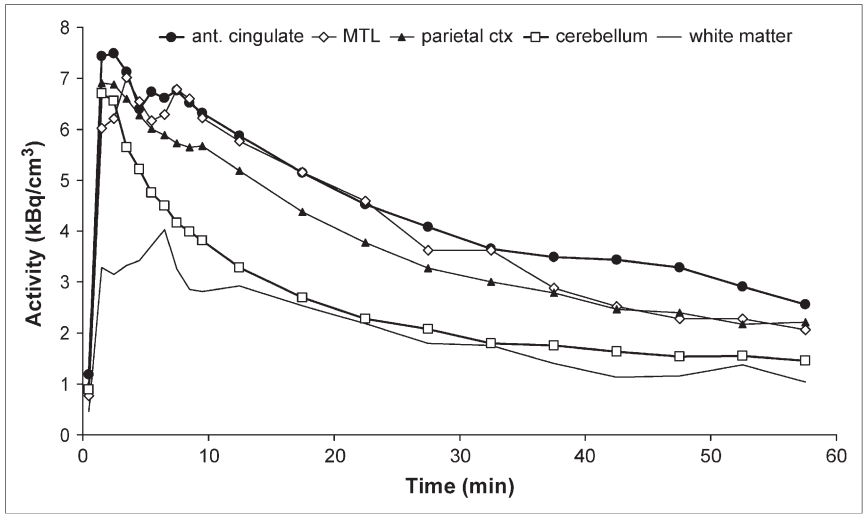

FIGURE 3. Time–activity curves of ^{11}C-ABP688 uptake in a single subject. Metabolite-corrected arterial activity was used as input function for calculating curves. Relatively high radioactivity concentrations were observed in mGluR5-rich brain regions such as anterior cingulate and medial temporal lobe, whereas radioactivity uptake in cerebellum and white matter, regions known to contain low densities of mGluR5, was low. ant = anterior; MTL = medial temporal lobe; ctx = cortex.

the blood–brain barrier. For central nervous system PET ligands, a log D value of between 2 and 3 has been postulated as an optimal range for good blood–brain barrier penetration (*25*). Time–activity curves (Fig. 3) revealed high radioactivity accumulation in mGluR5-rich regions such as the anterior cingulate, caudate, putamen, amygdala, and medial temporal lobe, with moderate binding in the thalamus and in the occipital and parietal cortical regions and a very low uptake in the cerebellum, in accordance with previous rodent studies (*18*).

Preliminary kinetic analysis demonstrated that a 2-tissue-compartment analysis is an appropriate approach to assess

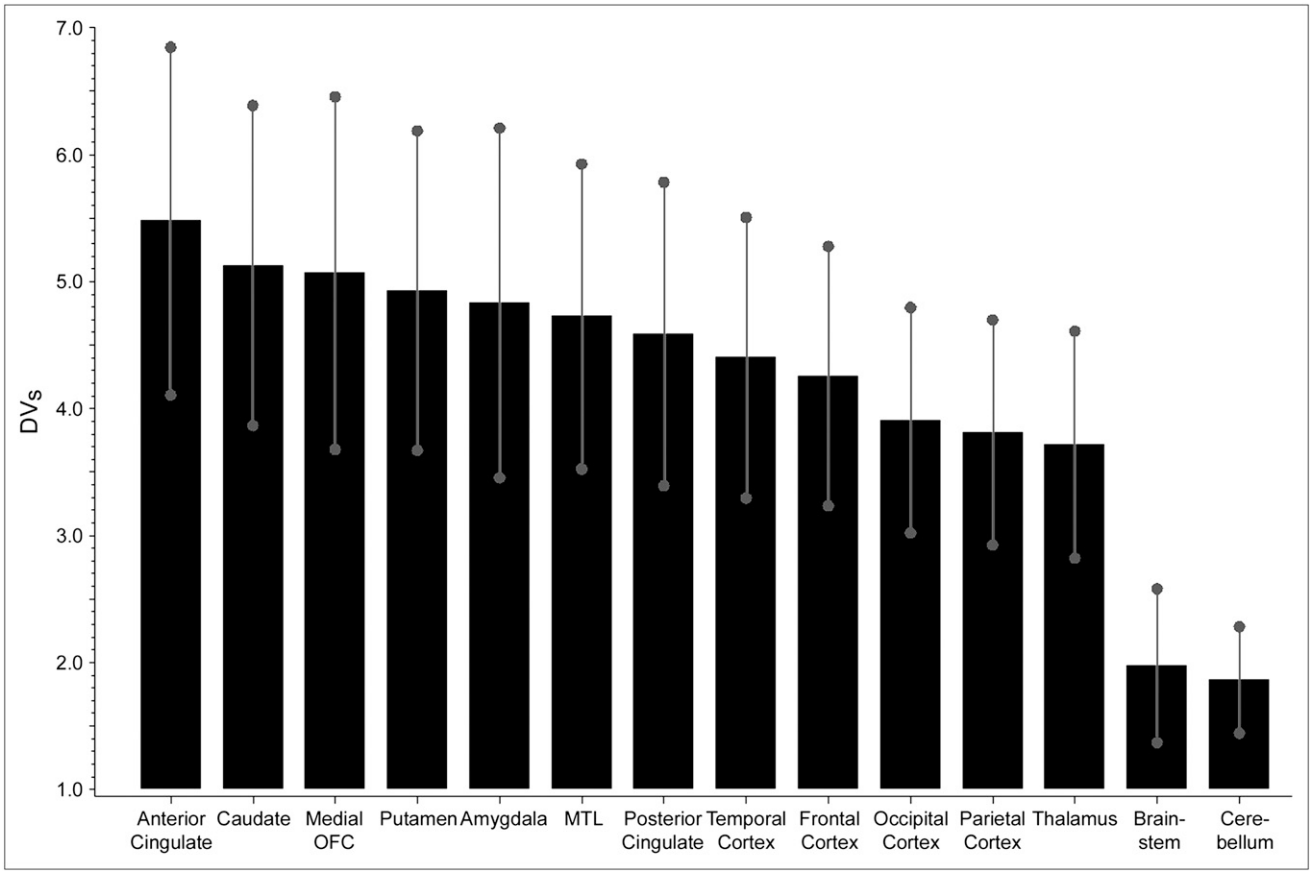

FIGURE 4. Specific DVs of ^{11}C-ABP688 uptake in various brain regions as outcome measure for mGluR5 density in human brain. Shown are mean values ± SD (n = 6). OFC = orbital frontal cortex; MTL = medial temporal lobe.

the specific DV of ^{11}C-ABP688 as a measure of receptor density. Except for white matter, all brain regions examined were best described by a 2-tissue-compartment model. The pattern of parametric images of the specific DVs was different from the perfusion studies with ^{15}O-H_2O and the K1 parametric images, indicating that this outcome measure of mGluR5 density is not perfusion-related. The rank order of the specific DVs obtained was in accordance with the reported distribution pattern of mGluR5 in rodents and humans (*26–28*). In a recent publication, Hamill et al. (*17*) described 3 potential PET ligands and their characterization in rhesus monkey brain. In this study, all 3 candidates exhibited selective uptake in mGluR5-rich regions such as the frontal cortex, striatum, and surprisingly the cerebellum, a brain region that has been shown to have a low or no expression of mGluR5 in rodents and humans (*26–28*). In the present study, the lowest DV was clearly in the cerebellum, a finding that is consistent with a low mGluR5 density. However, the exact fraction of specific DV in the cerebellum would have to be determined with a blocking study. Whether such a blocking study, which would require substantial doses of a blocking agent, can be performed on humans is not clear. An alternative could be to perform in vitro autoradiography using postmortem human brain tissue. Nevertheless, the higher specific DVs obtained in brain regions known to contain high densities of mGluR5, the lower cerebellar uptake, and the good agreement of the present data with previous rodent studies (*18*) suggest that radioactivity uptake in these brain regions reflects the pattern of mGluR5 distribution in humans.

In the radiometabolite analysis, the extraction method proved suitable, because the recovery of radioactivity was greater than 92%. Radiolabeled metabolites were more hydrophilic than the parent compound and thus were unlikely to cross the blood–brain barrier. Previous animal studies showed that more than 95% of radioactivity in rat brain 30 min after injection consisted of unchanged ^{11}C-ABP688. Although the radiolabeled metabolites were not identified, the metabolite profile suggests a similar metabolic fate of ^{11}C-ABP688 in both rodents and humans.

CONCLUSION

An efficient radiosynthesis for producing ^{11}C-ABP688 in good radiochemical yield and with high specific radioactivity for application in humans was developed. The highest uptake of ^{11}C-ABP688 was in mGluR5-rich regions such as the anterior cingulate, medial temporal lobe, putamen, and caudate. The specific DVs calculated from several regions of interest also agreed well with prior animal data. Taken together, these data suggest that ^{11}C-ABP688 has suitable characteristics for exploring mGluR5 distribution in humans using PET. Furthermore, ^{11}C-ABP688 could be of great value for the selection of appropriate doses of clinically relevant candidate drugs that bind to the mGluR5 and for PET studies on patients with psychiatric and neurologic disorders.

ACKNOWLEDGMENTS

We acknowledge the support of Pius August Schubiger, the head of the Center for Radiopharmaceutical Science of ETH, PSI, and USZ; René Amstutz, the head of Discovery Technologies; and Graeme Bilbe, the head of the Neuroscience Department at the Novartis Institutes for Biomedical Research. We also thank Cyril Burger, Christoph Hock, and Andrea Bettio for their contributions.

REFERENCES

1. Pin JP, Duvoisin R. The metabotropic glutamate receptors: structure and functions. *Neuropharmacology.* 1995;34:1–26.
2. Spooren WP, Gasparini F, Salt TE, Kuhn R. Novel allosteric antagonists shed light on mGluR5 and CNS disorders. *Trends Pharmacol Sci.* 2001;22:331–337.
3. Gereau RW, Conn PJ. Roles of specific metabotropic glutamate receptor subtypes in regulation of hippocampal CA1 pyramidal cell excitability. *J Neurophysiol.* 1995;74:122–129.
4. Spooren WP, Vassout A, Neijt HC, et al. Anxiolytic-like effects of the prototypical metabotropic glutamate receptor 5 antagonist 2-methyl-6-(phenylethynyl)-pyridine in rodents. *J Pharmacol Exp Ther.* 2000;295:1267–1275.
5. Tatarczynska E, Klodzinska A, Chojnacka-Wojcik E, et al. Potential anxiolytic- and antidepressant-like effects of MPEP, a potent, selective and systemically active mGlu5 receptor antagonist. *Br J Pharmacol.* 2001;132:1423–1430.
6. Ohnuma T, Augood SJ, Arai H, McKenna PJ, Emson PC. Expression of the human excitatory amino acid transporter 2 and metabotropic glutamate receptors 3 and 5 in the prefrontal cortex from normal individuals and patients with schizophrenia. *Brain Res Mol Brain Res.* 1998;56:207–217.
7. Rouse ST, Marino MJ, Bradley SR, Awad H, Wittmann M, Conn PJ. Distribution and roles of metabotropic glutamate receptors in the basal ganglia motor circuit: implications for treatment of Parkinson's disease and related disorders. *Pharmacol Ther.* 2000;88:427–435.
8. Chiamulera C, Epping-Jordan MP, Zocchi A, et al. Reinforcing and locomotor stimulant effects of cocaine are absent in mGluR5 null mutant mice. *Nat Neurosci.* 2001;4:873–874.
9. Walker K, Bowes M, Panesar M, et al. Metabotropic glutamate receptor subtype 5 (mGluR5) and nociceptive function. I. Selective blockade of mGluR5 in models of acute, persistent and chronic pain. *Neuropharmacology.* 2001a;40:1–9.
10. Walker K, Reeve A, Bowes M, et al. MGluR5 and nociceptive function II. MGluR5 functionally expressed on peripheral sensory neurones mediate inflammatory hyperalgesia. *Neuropharmacology.* 2001b;40:10–19.
11. Sotgiu ML, Bellomi P, Biella GE. The mGluR5 selective antagonist 6-methyl-2-(phenylethynyl)-pyridine reduces the spinal neuron pain-related activity in mononeuropathic rats. *Neurosci Lett.* 2003;342:85–88.
12. Gasparini F, Andres H, Flor PJ, et al. ^{3}H-M-MPEP, a potent subtype selective radioligand for the metabotropic glutamate receptor subtype 5. *Bioorg Med Chem Lett.* 2002;12:407–409.
13. Patel S, Krause SM, Hamill T, Chaudhary A, Burns HD, Gibson RE. In vitro characterization of ^{3}H-methoxyPEPy, an mGluR5 selective radioligand. *Life Sci.* 2003;73:371–379.
14. Gasparini F, Lingenhohl K, Stoehr N, et al. 2-Methyl-6-(phenylethynyl)-pyridine (MPEP), a potent, selective and systemically active mGluR5 antagonist. *Neuropharmacology.* 1999;38:1493–1503.
15. Ametamey SM, Kessler L, Honer M, et al. Radiosynthesis and preclinical evaluation of ^{11}C-ABP688 as a probe for imaging metabotropic glutamate receptor subtype 5 (mGluR5). *J Nucl Med.* 2006;47:698–705.
16. Kokic M, Honer M, Ametamey SM, et al. Radiolabeling and in vivo evaluation of ^{11}C-M-MPEP as a PET ligand for imaging the metabotropic glutamate receptor 5 (mGluR5). *J Labelled Compds Radiopharm.* 2001;44:231.
17. Hamill TG, Krause S, Ryan C, et al. Synthesis, characterization, and first successful monkey imaging studies of metabotropic glutamate receptor subtype 5 (mGluR5) PET radiotracers. *Synapse.* 2005;56:205–216.
18. Ametamey SM, Kessler LJ, Honer M, et al. Radiosynthesis and preclinical evaluation of ^{11}C-ABP688 as a probe for imaging the metabotropic glutamate receptor subtype 5. *J Nucl Med.* 2006;47:698–705.

19. Schönbächler R, Ametamey SM, Schubiger PA. Synthesis and ^{11}C-radiolabelling of a tropane derivative lacking the 2β-ester group: a potential tracer for the dopamine transporter. *J Labelled Compds Radiopharm.* 1999;42:447–456.
20. Mikolajczyk K, Szabatin M, Rudnicki P, Grodzki M, Burger CA. JAVA environment for medical image data analysis: initial application for brain PET quantitation. *Med Inform (Lond).* 1998;23:207–214.
21. Alpert NM, Eriksson L, Chang JY, et al. Strategies for the measurement of regional cerebral flow using short-lived tracers and emission tomography. *J Cereb Blood Flow Metab.* 1984;4:28–34.
22. Buck A, Westera G, vonSchulthess G, Burger C. Modeling alternatives for cerebral carbon-11 iomazenil kinetics. *J Nucl Med.* 1996;37:699–705.
23. Koeppe RA, Frey KA, Snyder SE, Meyer P, Kilbourn MR, Kuhl DE. Kinetic modeling of N-[^{11}C]methylpiperidin-4-yl propionate: alternatives for analysis of an irreversible positron emission tomography trace for measurement of acetylcholinesterase activity in human brain. *J Cereb Blood Flow Metab.* 1999;19:1150–1163.
24. Akaike H. A new look at the statistical model identification. *IEEE Trans Automat Contr.* 1974;AC19:716–723.
25. Wilson AA, Houle S. Radiosynthesis of carbon-11 labeled N-methyl 2-(arylthio)benzylamines: potential tracers for the serotonin reuptake receptor. *J Labelled Compds Radiopharm.* 1999;42:1277–1288.
26. Romano C, Sesma MA, McDonald MT, O'Malley K, Van den Pol AN, Olney JW. Distribution of metabotropic glutamate receptor 5 (mGluR5) immunoreactivity in rat brain. *J Comp Neurol.* 1995;355:455–469.
27. Daggett LP, Sacaan AI, Akong M, et al. Molecular cloning and characterization of recombinant human metabotropic glutamate receptor subtype 5. *Neuropharmacology.* 1995;34:871–886.
28. Blumcke I, Behle K, Malitschek B, et al. Immunohistochemical distribution of metabotropic glutamate receptor subtypes mGluR1b, mGluR2/3, mGluR4a and mGluR5 in human hippocampus. *Brain Res.* 1996;736:217–226.